A&A 464, 953–965 (2007)
DOI: 10.1051/0004-6361:20066061

Astronomy & Astrophysics

Na-O anticorrelation and horizontal branches

V. The Na-O anticorrelation in NGC 6441 from Giraffe spectra⋆,⋆⋆

R. G. Gratton[1], S. Lucatello[1], A. Bragaglia[2], E. Carretta[2], S. Cassisi[3], Y. Momany[1], E. Pancino[2], E. Valenti[2,4], V. Caloi[5], R. Claudi[1], F. D'Antona[6], S. Desidera[1], P. François[7], G. James[8], S. Moehler[9], S. Ortolani[10], L. Pasquini[9], G. Piotto[10], and A. Recio-Blanco[11]

[1] INAF – Osservatorio Astronomico di Padova, Vicolo dell'Osservatorio 5,35122 Padova, Italy
e-mail: raffaele.gratton@oapd.inaf.it
[2] INAF – Osservatorio Astronomico di Bologna, via Ranzani 1, 40127 Bologna, Italy
[3] INAF – Osservatorio Astronomico di Teramo, via M. Maggini, 64100 Teramo, Italy
[4] Dipartimento di Astronomia, Università di Bologna, via Ranzani 1, 40127 Bologna, Italy
[5] Istituto di Astrofisica Spaziale e Fisica Cosmica, via Fosso del Cavaliere, 00133 Rome, Italy
[6] INAF – Osservatorio Astronomico di Roma, via Frascati 33, 00040 Monteporzio, Italy
[7] Observatoire de Paris-Meudon, 5 place Jules Janssen, 92195 Meudon, France
[8] European Southern Observatory, 3107 Alonso de Cordova, Vitacura, Casilla 19001, Santiago 19, Chile
[9] European Southern Observatory, Karl-Schwarzschild-Strasse 2, 85748 Garching bei Munchen, Germany
[10] Dipartimento di Astronomia, Università di Padova, Vicolo dell'Osservatorio 2, 35122, Padova, Italy
[11] Observatoire Astronomique de la Côte d'Azur, Boulevard de l'Observatoire, BP 4229, 06304 Nice Cedex 4, France

Received 18 July 2006 / Accepted 22 December 2006

ABSTRACT

Aims. We present an analysis of FLAMES-Giraffe spectra for several bright giants in NGC 6441, to investigate the presence and extent of the Na-O anticorrelation in this anomalous globular cluster.
Methods. The field of NGC 6441 is very crowded, with severe contamination by foreground (mainly bulge) field stars. Appropriate membership criteria were devised to identify a group of 25 likely cluster members among the about 130 stars observed. Combined with the UVES data obtained with the same observations (Gratton et al. 2006), high dispersion abundance analyses are now available for a total of 30 stars in NGC 6441, 29 of them having data for both O and Na. The spectra were analyzed by a standard line analysis procedure; care was taken to minimize the impact of the differential interstellar reddening throughout the cluster, and to extract reliable information from crowded, and moderately high *S/N* (30–70), moderately high resolution ($R \sim 23\,000$) spectra.
Results. NGC 6441 has the typical abundance pattern seen in several other globular clusters. It is very metal-rich ([Fe/H] = $-0.34 \pm 0.02 \pm 0.04$ dex). There is no clear sign of star-to-star scatter in the Fe-peak elements. The α-elements Mg, Si, Ca, and Ti are overabundant by rather large factors, suggesting that the cluster formed from material enriched by massive core collapse SNe. The O-Na anticorrelation is well defined, with about 1/4 of the stars being Na-rich and O-poor. One of the stars is a Ba-rich and moderately C-rich star. Such stars are rare in globular clusters.
Conclusions. The distribution of [Na/O] ratios among RGB stars in NGC 6441 appears similar to the distribution of colors of stars along the horizontal branch. The fraction of Na-poor, O-rich stars found in NGC 6441 agrees well with that of stars on the red horizontal branch of this cluster (in both cases about 80%), with a sloping distribution toward lower values of [O/Na] (among RGB stars) and bluer colors (among HB stars).

Key words. stars: abundances – stars: atmospheres – stars: Population II – Galaxy: globular clusters: general – Galaxy: globular clusters: individual: NGC 6441

1. Introduction

Extensive studies by several groups during the last decades have shown that globular clusters (GCs) have a peculiar pattern in their chemical abundances. While they generally are very homogeneous insofar Fe-peak elements are concerned, they very often (possibly always) exhibit large star-to-star variations in the abundances of the light elements (see Gratton et al. 2004). The most prominent feature is the presence of anticorrelations between the abundances of various elements: C and N, Na and O, Mg and Al. These anticorrelations are attributed to the presence at the stellar surfaces of a fraction of the GC stars of material which has been processed by H burning at temperatures of a few tens million K. At this temperature, H-burning occurs through the CNO cycle, so that the abundance pattern of these elements is shifted toward the equilibrium values, which means enhanced N and depleted C and O abundances. At the same temperatures, proton captures on Ne and Mg produce large amounts of Na and Al (Denissenkov & Denissenkova 1990; Langer et al. 1993), so that the whole pattern of anticorrelations is present. This pattern is typical of GC stars; field stars only show changes in C and N abundances expected from typical evolution of low mass stars (Gratton et al. 2000; Sweigart & Mengel 1979; Charbonnel 1994). It is now

⋆ Based on data collected at the European Southern Observatory with the VLT-UT2, Paranal, Chile (ESO Program 073.D-0211).

⋆⋆ Full Table 3 is only available in electronic form at the CDS via anonymous ftp to cdsarc.u-strasbg.fr (130.79.128.5) or via http://cdsweb.u-strasbg.fr/cgi-bin/qcat?J/A+A/464/953

well accepted that the abundance pattern seen in GC stars is primordial, since it is observed in stars at all evolutionary phases (Gratton et al. 2001, and several other references cited in Gratton et al. 2004).

Since high Na and low O abundances are the signatures of material processed through hot H-burning, we expect that this abundance anomaly be accompanied by high He-contents. D'Antona & Caloi (2004) estimated an He excess of $\Delta Y \sim 0.04$ for the Na-rich, O-poor stars. Values of $\Delta Y \sim 0.15$ have been recently suggested to justify the observed sequences in NGC 2808 (D'Antona et al. 2005). While such a difference in the He-content should have small impact on the colors and magnitudes of stars up to the tip of the red giant branch (RGB hereafter), a large impact is expected on the colors of the horizontal branch (HB) stars: He-rich stars should be less massive by about 0.05 $M_{\odot}$. In the case of GCs of intermediate metallicity ([Fe/H] ~ -1.5), the expectation is then that the progeny of He-rich, Na-rich, O-poor RGB stars should reside on the blue part of the HB (i.e. bluer than the RR Lyrae instability strip), while the progeny of the "normal" He-poor, Na-poor, O-rich stars would fall within or redward of the instability strip. When comparing different clusters, the actual pattern may be more complicated, since small age differences of ∼2−3 Gyr may also cause different mean colors for the HB stars. However, within a single cluster it is expected that there should be a correlation between the distribution of masses (i.e. colors) of the HB-stars and the distribution of Na and O abundances. Note that star-to-star variable mass loss is a possibility, possibly fudging the correlation.

In this respect, GCs of high metallicity are of great interest. In the scenario devised by D'Antona & Caloi (2001) the He-poor, O-rich, Na-poor stars should lie on the red side of the RR Lyrae instability strip; i.e. these clusters should have a red HB. However, if the cluster age is large, He-rich, O-poor, Na-rich stars might fall within the instability strip or even be bluer than that, while in somewhat younger clusters, even He-rich stars would be on the red HB. Several metal-rich GCs, including the archetypes 47 Tuc and M 71, indeed show short red HBs, even though they also exhibit a clear O-Na anticorrelation. However, they are probably about 2 Gyr younger than the oldest GCs (see Rosenberg 1999; Gratton et al. 2003a; De Angeli et al. 2005). There are however two other metal-rich GCs (NGC 6388 and NGC 6441) which show very different HBs: while most of the stars still lie on the red side of the HB, both clusters have a large population of blue HB stars (Rich et al. 1997). It is very tempting to correlate this feature with the presence of He-rich stars, that could also explain the fact that the blue HB is brighter than the red HB (Sweigart & Catelan 1998), coupled with a rather old age[1]. Age determinations for these clusters require analyses of deep color–magnitude diagrams (CMDs hereafter), and it is complicated by the fact that both are projected toward the central regions of our Galaxy, so that they are severely contaminated by field stars and affected by large and variable interstellar absorption. On the other hand, it would be extremely interesting to study the Na-O anticorrelation in these clusters.

To check if the scenario by D'Antona & Caloi is acceptable, we have undertaken an extensive study of the O-Na anticorrelation in several GCs, with the purpose of determining as accurately as possible the distribution of stars along this anticorrelation. We expect that this distribution reflects a distribution in He abundances, hence in masses for RGB and HB stars. In this study we exploit the possibility to obtain high resolution spectra for large number of stars offered by the FLAMES multifibre facility at VLT-UT2 (Pasquini et al. 2002). With FLAMES, we may simultaneously obtain spectra of moderately high resolution ($R \sim 23\,000$) for more than a hundred stars using the Giraffe spectrograph, and higher resolution spectra ($R \sim 45\,000$) with larger spectral coverage of up to 8 stars with the UVES spectrograph. This instrument is then ideal for the present purposes. Early results from this survey, concerning the intermediate metal-poor clusters NGC 2808 and NGC 6752, were already presented by Carretta et al. (2006, 2007): the distributions of O-Na abundances derived for these two clusters closely match the distributions of stars along the HB. However, more data are clearly needed before sound conclusions can be drawn. We included in our survey also NGC 6388 and NGC 6441. The results from the UVES spectra of the latter were presented in Gratton et al. (2006, hereinafter Paper II): NGC 6441 is metal rich ([Fe/H] $= -0.39 \pm 0.02 \pm 0.04$), and overabundant in the α-elements. We also found that one of the five stars member of the cluster has Na and O abundances distinctly different (respectively higher and lower for Na and O) from the remaining four. In the present paper, we present the analysis of the Giraffe spectra. While these spectra have lower resolution and cover narrower spectral ranges than those obtained with UVES, the much larger number of stars observed gives the opportunity of a better discussion of the distribution of stars along the O-Na anticorrelation. Unluckily, the large number of contaminating field stars (which could not be excluded a priori due to the lack of an appropriate membership study before our observations were carried out) limited the observed sample to a total of 25 stars which are bona fide members of NGC 6441 that we combined with the five bona fide members observed with UVES. While this is not enough for a detailed comparison like that performed by Carretta et al. (2006, 2007) for the much easier clusters NGC 2808 and NGC 6752, it is still enough to give a first sketch of the distribution.

This paper is organized as follows: in Sect. 2 we describe the observational data. In Sect. 3 we discuss the radial velocities and the cluster membership. In Sect. 4 we present the abundance analysis for the stars found to be members of the cluster, in Sect. 5 we discuss our results and we compare the abundance distributions with other cluster properties. In Sect. 6 we comment about one particular star member of NGC 6441, that belongs to the class of Ba-rich stars, quite rare among GCs. Finally, conclusions are drawn in Sect. 7.

2. Observations and data reduction

Observations of NGC 6441 are described in detail in Paper II; we give here only a few details relevant for the present purposes. Observations were done with two Giraffe setups, the high-resolution gratings HR11 (centered at 5728 Å) and HR13 (centered at 6273 Å) to measure the Na doublets at 5682–88 Å and 6154–6160 Å, and the [OI] forbidden lines at 6300, 6363 Å, respectively. Resolution at the center of spectra is $R = 24\,200$ (for HR11) and $R = 22\,500$ (for HR13). We have a total exposure time of 15 900 s for HR11 and 10 600 s for HR13: the latter were however obtained in better observing conditions, so that the spectra obtained with HR13 were of higher *S/N*.

Our targets were selected among isolated RGB stars, using the photometry described in Paper II. Criteria used to select the stars are described at length in Paper II. Not all the stars were

[1] A high He content for the blue HB stars of NGC 6388 is supported by the results of Moehler & Sweigart (2006).

Table 1. Journal of observations.

Grating Configuration	Date	Time	Exp. time (s)	Seeing (arcsec)	Airmass
HR11	2004-07-06	04:21:42	5300	1.59	1.040–1.174
	2004-07-11	02:48:19	5300	1.35	1.029–1.052
	2004-07-11	04:19:18	5300	0.91	1.055–1.221
HR13	2004-07-17	05:18:20	5300	0.69	1.202–1.605
	2004-07-26	03:39:54	5300	1.04	1.077–1.282

observed with both gratings; on a grand total of 127 stars (25 cluster members: see below for the adopted membership criteria), we have 97 objects (15 cluster members) with spectra for both gratings, 19 (1 cluster member) with only HR11 observations, and 21 (9 cluster members) with only HR13 observations. Since the Na doublet at 6154–60 Å falls into the spectral range covered by HR13, we could measure Na abundances for all target stars, whereas we could expect to measure O abundances only up to a maximum of 118 stars (24 cluster members). Table 1 lists information about the two pointings.

Table 2 gives details on the main parameters for the member stars (see next section for the adopted membership criteria). Star designations are according to the photometry described in Paper II, from which photometric data were also taken. Coordinates (at J2000 equinox) are from our astrometry; distances from the cluster center were obtained considering the nominal position given by Harris (1996). The signal-to-noise ratios *S/N* were estimated from the pixel-to-pixel scatter in spectral regions relatively free from absorption lines; however, since spectral regions truly free from absorption features are virtually nonexistent in these spectra, we adopted this method after dividing each spectrum by an average spectrum obtained summing the spectra of all stars members of the cluster. The V, $V-I$. CMD of our sample is shown in Fig. 1 with overimposed an appropriate isochrone (13 Gyr, [Fe/H] = −0.32) from Pietrinferni et al. (2004), shifted by the distance modulus $(m-M)_V = 16.79$ (Harris catalog) and reddened adopting $E(B-V) = 0.49$. Our targets are in the range from about $V = 16.2$ to 17.2 and $V-I = 1.88$ to 2.32. The selected stars are well below the tip of the RGB and span the whole range in color of the broad RGB of NGC 6441.

We used the 1-d, wavelength calibrated spectra as reduced by the dedicated Giraffe pipeline (BLDRS v0.5.3, written at the Geneva Observatory, see `http://girlbirds.sourceforge.net`). The radial velocities (RVs) have been measured by the Giraffe pipeline, which performs a cross-correlation using an appropriate synthetic spectrum as a template. The typical errors on these measurements are around 0.3–0.5 km s^{-1}. Further analysis was done with IRAF[2]. We subtracted the background using 8 fibers dedicated to the sky, rectified the spectra, corrected for contamination by telluric features in the HR13 spectra using the task TELLURIC and shifted all the spectra to zero RV before summing all individual spectra for each stars.

3. Cluster membership

In order to properly define membership to the cluster, we first defined a parameter $p = \sqrt{(\mathrm{Dist}/300)^2 + ((RV-21.0)/12.5)^2}$, where Dist is the projected distance from the cluster center (in arcsec), and RV is the radial velocity in km s^{-1}, p represents the distance of each star from the cluster center mean position in the Dist − RV plane, roughly expressed in units of standard deviation of the distributions. Note that according to Harris (1996) the tidal radius of NGC 6441 is about 467 arcsec, and the average radial velocity is +16.4 ± 1.2 km s^{-1}; however the final values we adopted for the average radial velocity and its scatter were iteratively obtained from the average and rms scatter of the probable members identified in our sample. p is obviously related to the probability that a star is a member of the cluster. Assuming uniform distributions in both position and RVs (for this last, over the range ±190 km s^{-1} from the mean cluster velocity, corresponding to the observed spread in RVs), we would expect 0.46 field stars with $p < 1$, 3.24 with $1 < p < 2$, 6.39 with $2 < p < 3$, and 3.70 with $3 < p < 4$[3], while the observed numbers in these bins are 8, 18, 14, and 3 (where we included also stars observed with UVES): the excess of objects around the cluster position in the $Dist - RV$ plane is obvious. These numbers suggest that membership probability based on these criteria alone is ∼94% for $p < 1$, ∼82% for $1 < p < 2$, about a half for $2 < p < 3$, and smaller for larger values of p. Combining this datum with metallicity we may improve separation of likely members from field stars, of course with some risk of biasing the metallicity distribution. We then examined the chemical composition for all stars with $p < 5$: the results are graphically shown in Fig. 2. After inspection of this figure, we finally defined as likely members of NGC 6441 those stars with $p < 3.0$ and $-0.6 <$ [Fe/H] < -0.1. 25 stars passed this criterion. Note that we removed from the sample 1 star out of 8 with $p < 1$, 4 stars out of 18 with $1 < p < 2$, and 5 stars out of 14 with $2 < p < 3$, in quite good agreement with the expected number of field stars. All stars with $p < 2.5$ removed from the sample of likely members are much more metal rich than the cluster average; the field stars have a mean metallicity around [Fe/H] ∼ −0.1[4]. There might be some additional members of NGC 6441: this is suggested by the height of the peak in the radial velocity distribution around the cluster mean velocity (Fig. 3). However, their membership being doubtful, we prefer not to use them in our analysis. Note that all stars considered members or probable members of NGC 6441 in Paper II would be considered members, and all those considered as field stars would be field stars according to the criteria of the present paper[5].

The average radial velocity that we obtained from our 25 confirmed members is 21.0 ± 2.5 km s^{-1}, with a star-to-star

[2] IRAF is distributed by the National Optical Astronomical Observatory, which is operated by the Association of Universities for Research in Astronomy, under contract with the National Science Foundation.

[3] This value is smaller than for the preceding bin because the edge of the Oz-Poz field was reached at this distance.

[4] As noticed in Paper II, most of the field stars should belong to the bulge. The line of sight toward NGC 6441 passes at about 1.1 kpc from the cluster center. However, the field star average metallicity might be biased by the selection procedure adopted, and should not be taken as representative of the bulge metal abundance in the direction toward NGC 6441.

[5] The list of stars not members of NGC 6441 can be obtained upon request from the authors.

Table 2. Photometry and spectroscopic data for stars observed with Giraffe.

Star	Gratings	RA (degree)	Dec (degree)	Dist. (arcsec)	V (mag)	$V-I$ (mag)	$V-K$ (mag)	RV (km s^{-1})	S/N HR11	S/N HR13	$\sigma(EW)$ (mÅ)	[Fe/H]
6005198	11+13	267.3757	−37.0886	528	16.274	2.327	5.007	12.1	15	43	17.1	−0.41
6005934	11+13	267.3842	−37.2010	727	16.387	1.985	4.359	23.0	22	37	13.7	−0.42
6007741	11+13	267.4520	−37.0056	334	16.612	2.055	4.467	17.0		28	15.6	−0.25
6010149	11	267.4408	−37.1361	446	16.842	2.114	4.510	30.6	23		11.0	−0.17
6012768	13	267.4320	−37.1921	616	17.043	2.105		13.3		50	7.8	−0.42
7004955	13	267.5810	−37.0124	160	16.232	2.164	4.783	11.4		69	10.0	−0.22
7006255	11+13	267.5414	−37.0654	62	16.430	1.998		13.3	33	50	8.3	−0.39
7006305	11+13	267.6267	−37.0145	248	16.437	2.112	4.576	27.0	34	65	9.8	−0.29
7006319	11+13	267.5162	−37.0608	113	16.438	1.975	4.483	6.5	45	58	11.4	−0.29
7006354	13	267.5631	−37.1049	196	16.442	2.261	4.842	32.4		53	9.8	−0.41
7006377	11+13	267.5129	−37.1338	320	16.445	2.105	4.646	13.5	41	55	6.5	−0.37
7006470	11+13	267.5570	−36.9669	303	16.458	1.946	4.423	0.9	31	55	9.9	−0.29
7006590	11+13	267.4963	−37.0236	192	16.475	1.877		4.3	30	50	10.1	−0.41
7006935	11+13	267.5364	−36.9426	394	16.518	2.143	4.687	18.9	42	57	8.0	−0.43
7006983	11+13	267.6414	−36.9409	470	16.522	2.075	4.441	27.8	42	57	6.8	−0.23
7007064	11+13	267.5956	−37.0473	122	16.535	2.304	4.953	29.1	49	66	10.1	−0.45
7007118	13	267.5242	−36.9683	310	16.542	1.978	4.367	18.9		64	5.7	−0.35
7007884	13	267.5766	−37.0884	150	16.631	2.061	4.955	28.2		64	11.6	−0.31
7008891	13	267.5674	−37.0043	173	16.730	1.989	4.312	13.6		54	7.8	−0.30
7013582	13	267.6406	−36.9898	334	17.097	2.145	4.586	17.8		53	7.4	−0.35
8005158	13	267.7439	−36.9866	594	16.267	2.013	4.480	36.8		51	8.3	−0.40
8005404	11+13	267.6974	−37.1418	527	16.306	2.228	4.894	48.4	26	59	12.3	−0.42
8006535	11+13	267.6661	−36.9818	408	16.467	2.240	4.973	8.1	33	88	10.8	−0.25
8008693	11+13	267.6896	−36.9899	449	16.711	2.272	4.850	25.0	34	32	25.8	−0.30
8013657	13	267.7280	−37.1704	660	17.103	2.111	4.632	44.0		41	6.8	−0.27

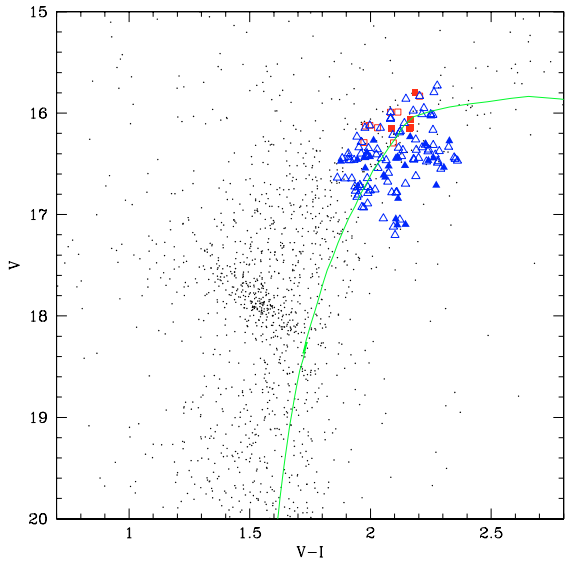

Fig. 1. (V, $V-I$) color magnitude diagram for selected stars in the field of NGC 6441 (from Valenti et al. 2006). Squares indicate stars observed with FLAMES-UVES, while triangles are the stars targeted by FLAMES-Giraffe. Filled symbols mark stars member of the cluster on the basis of RVs and location in the field close to the cluster center; open symbols are non-member stars. Overimposed is an isochrone computed for an age of 13 Gyr and [Fe/H] = −0.32 from Pietrinferni et al. (2004). This isochrone is for a solar scaled composition.

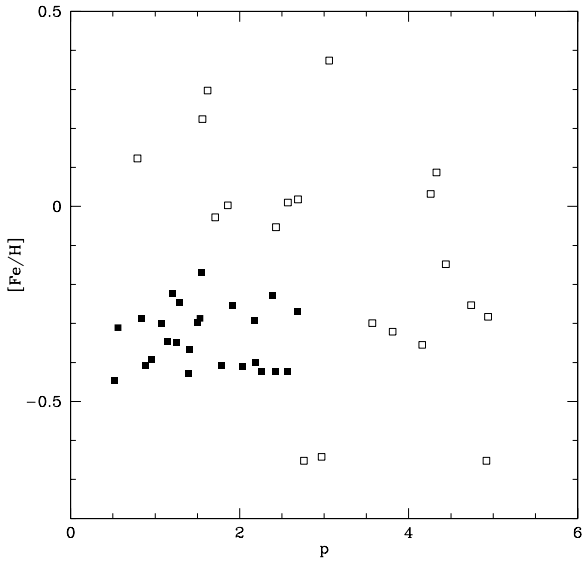

Fig. 2. Derived iron abundance as a function of the p parameter (see text for definition) for the analyzed stars. Filled symbols are likely members, open symbols are non members.

rms scatter of 12.5 km s^{-1}. If we add the five stars members of the cluster observed in Paper II, the average radial velocity is the same, and the rms scatter increases to 13.2 km s^{-1}. The observed radial velocity scatter, although quite large, is not surprising for this cluster, which is known to have a very large central velocity dispersion (see e.g. Illingworth 1979; Dubath et al. 1997) The observed mean radial velocity value is slightly larger than that given by Harris (1996); this might be due to some contamination by the field stars in some of the literature determinations used by Harris, since on average field stars have a negative radial velocity of ∼−50 km s^{-1} (see Fig. 3), in agreement with the expected values for this direction on the basis of the bulge rotation curve by Tiede & Tendrup (1997; see also Côté 1999).

Table 3. Equivalent Widths from Giraffe spectra. The full data is available in electronic form at the CDS.

El	Wavel. (Å)	E.P. (eV)	log *gf*	6005198 (mÅ)	6005934 (mÅ)	6007741 (mÅ)	6010149 (mÅ)	6012768 (mÅ)	7004955 (mÅ)	7006255 (mÅ)	7006305 (mÅ)	7006319 (mÅ)	7006354 (mÅ)
8.1	6300.31	0.00	–9.75	45.0	54.0	0.0	0.0	0.0	36.5	0.0	57.4	44.0	56.0
8.1	6363.79	0.02	–10.25	38.0	28.0	14.0	0.0	16.0	0.0	11.0	18.0	29.0	36.0
11.1	6154.23	2.10	–1.57	126.7	78.4	117.8	0.0	83.4	163.3	116.3	122.3	74.6	114.7
11.1	6160.75	2.10	–1.26	141.0	103.7	133.4	0.0	0.0	182.8	147.2	139.4	102.6	126.2
12.1	5711.09	4.34	–1.71	0.0	124.8	0.0	154.0	0.0	0.0	113.5	158.6	143.0	0.0

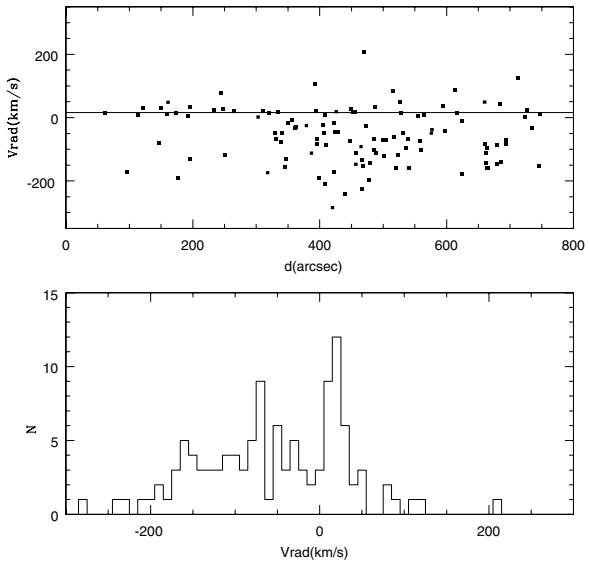

Fig. 3. *Upper panel*: RV vs. distance from the cluster center (in arcsec) for all the observed stars. *Lower panel*: radial velocity histogram for all the observed stars. The excess of stars at $RV \sim +20$ km s^{-1} corresponds to the average velocity of NGC 6441; this is represented as a solid line in the upper panel.

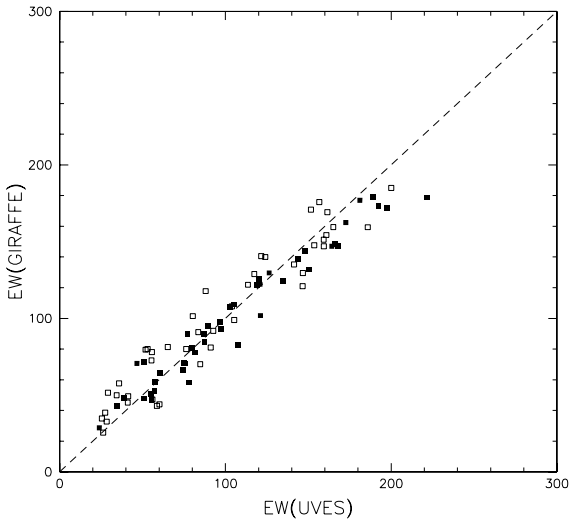

Fig. 4. Comparison between the *EW*s derived from Giraffe and UVES spectra for the two stars which were observed in both modes. Filled symbols are for star #6003734; open symbols are for star #7004329.

4. Abundance analysis

4.1. Equivalent widths

The equivalent widths (*EW*s) were measured using the ROSA code (Gratton, private communication; see Table 3 for stars members of NGC 6441) with Gaussian fittings to the measured profiles: these exploit a linear relation between *EW*s and FWHM of the lines, derived from a subset of lines characterized by cleaner profiles (see Bragaglia et al. 2001 for further details on this procedure). Since the observed stars span a very limited atmospheric parameter range ($3908 \leq T_{\rm eff} \leq 4321$ K and $1.26 \leq \log g \leq 1.74$), internal errors in these *EW*s may be estimated by comparing measures for individual stars with the average values over the whole sample: the values given in Col. 10 of Table 2 are the rms of residuals around a best fit line, after eliminating a few outliers. These errors may be slightly overestimated, due to real star-to-star differences. They are roughly reproduced by the formula $\sigma(EW) \sim 416/(S/N)$ mÅ. Considering the resolution and sampling of the spectra, the errors in the *EW*s are about 1.3 times larger than expectations based on photon noise statistics (Cayrel 1988 – considering that we used only the inner part of the profile when deriving the equivalent widths), showing that a significant contribution to errors is due to uncertainties in the correct positioning of the continuum level; the observed errors could be justified by errors of slightly less than 1% in the estimate of the correct continuum level.

Tests on possible systematic errors in the *EW*s may be done by comparing them with those from other data sets. We could perform this analysis for two stars (#6003734 and #7004329) having both UVES and Giraffe spectra (taken on different observing set ups). Both stars are not members of NGC 6441. On average the *EW*s measured on the Giraffe spectra are larger than those measured on the UVES spectra by 0.3 ± 1.6 mÅ, with an rms scatter of 14.5 mÅ (see Fig. 4 for a graphical comparison). The regression line through the points in this figure is *EW*(GIRAFFE) = (0.84 ± 0.03) *EW*(UVES) + (16 ± 12) mÅ. While the scatter agrees with expected errors on both sets of *EW*s, the regression line suggests that the *EW*s in the GIRAFFE spectra can be overestimated for the weaker lines and underestimated for the strong ones. However, we deem this result too uncertain to apply any systematic correction to the present *EW*s. The impact of this potential error on the derived abundances will be commented later on in the text.

4.2. Atmospheric parameters

We performed a standard line analysis on the equivalent widths measured on our spectra, using model atmospheres extracted by interpolation from the grid by Kurucz (1992; models with the overshooting option switched off). Atmospheric parameters defining these model atmospheres were obtained as follows.

Whenever possible, effective temperatures were derived from a calibration of *K* magnitudes, drawn from the 2MASS catalog (Skrutskie et al. 2006). The idea is quite simple: our purpose is to derive the most accurate temperatures from individual stars

in a case where the dominant source of error for temperatures derived from photometry is differential reddening. We may accept a scale error (that is a zero point error common to all stars), but we wish to reduce the star-to-star error. K magnitudes are much less affected by reddening than $V - K$ colors. Hence, if the dominant source of error is differential reddening, the best solution would be to have a relation where we enter K magnitudes and retrieve the corresponding $T_{\rm eff}$ values. This is possible in a cluster insofar we may assume that there is a unique relation between luminosity and effective temperature, which is a reasonable assumption along the RGB if all cluster stars have the same metallicity (see below).

In principle, we would need a different $K - T_{\rm eff}$ relation for each star, because of differential reddening; however, this individual $K - T_{\rm eff}$ relation is very close to the average one over all cluster stars, because the impact of differential reddening on K magnitudes is very limited. In fact, roughly speaking, $A(K) = 0.4\ E(B-V)$, hence for a differential reddening rms of 0.05 mag (Layden et al. 1999; Pritzl et al. 2001), the different $K - T_{\rm eff}$ relations differ from the average one by some 0.02 mag rms; since the slope of the $K - T_{\rm eff}$ relation is 332 K/mag, the errors made by adopting a unique average relation rather than one appropriate for each star is $0.02 \times 332 = 7$ K. The internal errors in the temperatures of individual stars are actually larger, because the photometric errors in the 2MASS K magnitudes (∼0.03 mag) should also be taken into account: they cause an error of about 10 K in the adopted temperatures. While the two errors should be summed in quadrature, we conservatively simply added them and attribute an internal error of ±17 K to the individual $T_{\rm eff}$'s.

The problem of deriving accurate temperatures then reduces to the derivation of the average $K - T_{\rm eff}$ relation for the cluster. This is obtained by fitting a straight line through the $K - T_{\rm eff}(V-K)$ points[6], and it is obviously valid only for that cluster. Each individual $T_{\rm eff}(V-K)$ is the temperature for each star derived from the $V-K$ color, de-reddened adopting the average cluster reddening (the value we adopted is $E(B-V) = 0.49$, which is the average value between various literature determinations; see Paper II for a discussion; this was transformed into $E(V-K)$ using the formula $E(V-K) = 2.75\ E(B-V)$, Cardelli et al. 1989), and using the calibration by Alonso et al. (1999; we adopted the same average metal abundance for all stars when using Alonso et al. formulas); the uncertainty in this average value translates into a scale error, that is much larger than the error for the individual stars because in this case we have to use the $V - K$ color: since the mean interstellar reddening toward NGC 6441 is uncertain by about 0.05 mag in $E(B-V)$, that is 0.13 mag in $E(V-K)$, and the slope of the $T_{\rm eff}(V-K)$ relation is 488 K/mag, the zero point of our $T_{\rm eff}$ scale has an uncertainty of at least ±67 K. Note that there should also be an additional statistical contribution, related to the spread of differential reddening and the number of stars used, but this is practically negligible. This error bar does not include possible errors in the Alonso et al. (1999) calibration. We will not consider here this last error, since we intend to adopt the Alonso et al. calibration throughout the whole present series of papers.

Practically, a complication in this approach is that there are many field interlopers. Luckily, radial velocities and positions can be used to eliminate most of them. The relations we used are based on the bona fide cluster members alone.

[6] The rms scatter around this straight line is of about 80 K, which is consistent with a dispersion of 0.06 mag in the reddening values, to be compared with the 0.05 mag proposed by Layden et al. (1999) and Pritzl et al. (2001), on a much larger number of stars.

As mentioned above, a basic assumption behind this approach is that the intrinsic width of the RGB of the cluster is negligible: this implies that all stars share the same metal abundance. A consistency check can be obtained a posteriori, looking at the spread in metal abundances. We indeed found that the scatter in metallicities among cluster members is consistent with expectations based on internal errors alone. Hence we have no reason to think that there is a real spread in metal abundances among the stars of NGC 6441.

For a few stars lacking of the 2MASS photometric data we inferred the K magnitudes by deriving the $(V-K)$ color from our $(V-I)$ colors. The mean relation is $(V-K) = 0.479 + 1.952\ (V-I)$, derived from more than 250 stars spanning over 4 mag in $(V-K)$ colors; the rms scatter around this mean relation is of 0.098 mag in $(V-K)$. We could derive consistent temperatures also for these stars; in this case the error bars are larger (about 40 K), since errors in their K magnitudes are of about 0.1 mag.

We may compare these temperatures derived from colors with those that we could deduce from excitation equilibrium for Fe I lines. We found that temperatures derived from Fe I excitation equilibrium are lower by 41 ± 29 K, with an rms scatter for individual stars of 145 K on average. This small difference can be attributed to several causes (errors in the adopted temperature scale, inadequacies of the adopted model atmospheres, etc.). On the whole we do not deem this difference as important. On the other hand, the fair agreement between temperatures from colors and spectra supports the assumed reddening (actually the best guess would be for a value of $E(B-V) = 0.459 \pm 0.022$, slightly lower than the value adopted here).

Surface gravities were obtained from the location of the stars in the CMD. This procedure requires assumptions about the distance modulus (we adopted $(m-M)_V = 16.33$ from Harris 1996 for the cluster members), the bolometric corrections (from Alonso et al. 1999), and the masses (we assumed a mass of 0.9 $M_\odot$, close to the value given by isochrone fitting). Uncertainties in these gravities are small for cluster stars (we estimate internal star-to-star errors of about 0.02 dex, due to the effects of possible variations in the interstellar absorption of 0.05 mag in the K magnitude; and systematic errors of about 0.11 dex, dominated by systematic effects in the temperature scale).

We may compare these values for the surface gravities with those deduced from the equilibrium of ionization of Fe. On average, abundances from Fe II lines are 0.04 ± 0.06 dex larger than that derived from Fe I lines. The agreement is obviously very good, but it could be fortuitous because other sources of errors (overionization, model atmospheres, gf, etc.) may cause much larger effects than the mean offset measured. The star-to-star scatter in the residuals is quite large (0.30 dex) due to the very limited number of Fe II lines typically used in the analysis.

Microturbulence velocities $v_{\rm t}$ were determined by eliminating trends in the relation between expected line strength and abundances (see Magain 1984). For stars with less than 25 lines measured we generally adopted a value of 1.6 km s^{-1} (similar to the average of the other star), save for a few cases where obvious trends were present. Given the typical uncertainties in the slope of expected line strength vs. abundances, this would imply an expected random error in the microturbulence velocities of ±0.15 km s^{-1}. However, we warn the reader not to rely too much on our microturbulent values, because they are model dependent.

Finally, model metal abundances were set in agreement with the average derived Fe abundance. The adopted model atmosphere parameters are listed in Table 4.

Table 4. Atmospheric parameters, Fe I, II, Na and O abundances for stars observed with Giraffe.

Star	$T_{\rm eff}$ (K)	log g	[A/H]	$v_{\rm t}$ (km s^{-1})	n	Fe I [Fe/H]	rms	n	Fe II [Fe/H]	rms	[O/Fe]	[Na/Fe]
6005198	3908	1.26	−0.32	1.4	32	−0.41	0.23	2	−0.29	0.52	−0.08	0.65
6005934	4161	1.56	−0.32	1.4	33	−0.42	0.24	2	−0.36	0.14	0.08	0.17
6007741	4199	1.60	−0.32	1.7	20	−0.25	0.26	1	−0.95		−0.17	0.55
6010149	4262	1.67	−0.32	1.7	13	−0.17	0.18					
6012768	4304	1.73	−0.32	1.0	19	−0.42	0.20	2	0.00	0.75	−0.02	0.40
7004955	3968	1.33	−0.32	1.7	18	−0.22	0.18	1	−0.68		−0.39	1.01
7006255	4162	1.56	−0.32	1.6	34	−0.39	0.19	1	−0.98		−0.31	0.65
7006305	4105	1.49	−0.32	1.4	33	−0.29	0.21	2	−0.28	0.42	−0.05	0.70
7006319	4136	1.53	−0.32	1.4	34	−0.29	0.22	1	−0.06		0.01	0.12
7006354	4019	1.39	−0.32	1.6	18	−0.41	0.15	2	−0.19	0.22	0.04	0.40
7006377	4085	1.47	−0.32	1.8	33	−0.37	0.16	1	−0.44		−0.21	0.57
7006470	4163	1.56	−0.32	1.4	34	−0.29	0.21	2	−0.24	0.46	0.11	0.18
7006590	4247	1.66	−0.32	1.4	34	−0.41	0.20	1	0.13		0.02	−0.10
7006935	4095	1.48	−0.32	2.0	33	−0.43	0.16	2	−0.43	0.24	0.15	0.07
7006983	4178	1.58	−0.32	1.4	32	−0.13	0.17	1	−0.06		0.17	0.43
7007064	4013	1.38	−0.32	1.8	31	−0.45	0.21	2	−0.21	0.46	0.05	0.03
7007118	4209	1.61	−0.32	1.8	34	−0.35	0.18	2	−0.31	0.33	0.19	0.35
7007884	4044	1.42	−0.32	1.7	19	−0.31	0.20	2	−0.22	0.45	0.12	0.16
7008891	4290	1.71	−0.32	1.7	18	−0.30	0.17	2	−0.42	0.22	0.35	0.14
7013582	4321	1.74	−0.32	1.7	21	−0.35	0.18	2	−0.62	0.64	0.22	0.50
8005158	4081	1.46	−0.32	1.6	19	−0.40	0.18	2	0.19	0.17	0.09	0.28
8005404	3956	1.32	−0.32	1.6	33	−0.42	0.21	2	−0.03	0.23	0.13	0.10
8006535	3983	1.35	−0.32	1.6	33	−0.25	0.21	2	−0.30	0.59	−0.02	0.27
8008693	4105	1.49	−0.32	1.8	32	−0.30	0.42	2	0.12	0.39	−0.10	1.01
8013657	4308	1.73	−0.32	1.0	21	−0.27	0.17	2	−0.45	0.54	0.18	0.54

Table 5. Uncertainties in Fe abundances for stars observed with Giraffe.

Element	Average No. lines	$T_{\rm eff}$	log g	[A/H]	$v_{\rm t}$	EWs	Total Internal	Total Systematic
Variation		100	+0.30	+0.20	+0.20			
Internal		17	0.02	0.00	0.15	0.200		
Systematic		67	0.11	0.04	0.04			
[Fe/H]I	32.0	0.005	0.070	0.057	−0.112	0.035	0.080	0.037
[Fe/H]II	1.7	−0.195	0.198	0.091	−0.041	0.152	0.164	0.176
[O/Fe]	1.8	0.027	0.052	0.021	0.103	0.149	0.172	0.075
[Na/Fe]	2.0	0.092	−0.073	−0.060	0.040	0.141	0.150	0.095
[Mg/Fe]	2.5	−0.035	−0.014	−0.028	0.077	0.126	0.144	0.065
[Si/Fe]	4.9	−0.120	0.018	−0.010	0.089	0.090	0.120	0.093
[Ca/Fe]	3.9	0.116	−0.108	−0.037	−0.018	0.101	0.110	0.100
[Sc/Fe]	3.8	−0.031	0.055	0.014	0.048	0.103	0.115	0.057
[Ti/Fe]	1.0	0.170	−0.058	−0.020	−0.088	0.200	0.216	0.148
[V/Fe]	10.3	0.195	−0.070	−0.007	−0.100	0.062	0.109	0.138
[Cr/Fe]	2.9	0.145	−0.045	−0.020	−0.076	0.117	0.138	0.113
[Ni/Fe]	13.2	−0.043	0.025	−0.002	0.040	0.055	0.072	0.043
[Ba/Fe]	1.0	0.014	0.005	0.037	−0.057	0.200	0.208	0.092

4.3. Fe abundances

Individual [Fe/H] values are listed in Table 4. Reference solar abundances are as in Gratton et al. (2003b). Throughout our analysis, we use the same line parameters discussed in Gratton et al. (2003b); in particular, collisional damping was considered using updated constants from Barklem et al. (2000).

Table 5 lists the impact of various uncertainties on the derived abundances for the elements considered in our analysis. Variations in parameters of the model atmospheres were obtained by changing each of the parameters at a time for star #7006354, assumed to be representative of all the stars considered in this paper.

The first three rows of the table give the variation of the parameter used to estimate sensitivities, the internal (star-to-star) errors, and the systematic errors (common to all stars) in each parameter. The second column gives the average number of lines n used for each element. Columns 3–6 give the sensitivities of the abundance ratios to variations of each parameter. Column 7 gives the contribution to the error given by uncertainties in the EWs for individual lines: this is $0.200/\sqrt{n}$, where 0.200 is the error in the abundance derived from an individual line, as obtained by the median error over all the stars. The last two columns give the total internal and systematic errors, obtained by summing quadratically the contribution of the individual source of errors, weighted according to the errors appropriate for each parameter. For the systematic errors, the contribution due to equivalent widths and to microturbulence velocities (quantities derived from our own analysis), were divided by the square root of the number of cluster members observed. Note that this error

analysis does not include the effects of covariances in the various error sources, which are however expected to be quite small for the program stars.

Errors in Fe abundances from neutral lines are dominated by uncertainties in the microturbulent velocity. We estimate random errors of 0.091 dex, and systematic errors of 0.037 dex. From Table 4, the average Fe abundance from all stars of NGC 6441 is [Fe/H] = −0.34 ± 0.02 (error of the mean), with an rms scatter of 0.08 dex from 25 stars. Then, the first result of our analysis is that the metallicity of NGC 6441 is [Fe/H] = −0.34 ± 0.02 ± 0.04. This value agrees well, within the errors, with the average Fe abundance determined in Paper II ([Fe/H] = −0.39 ± 0.04 ± 0.05). The small difference could be explained by the trends in *EW*s discussed in Sect. 4.1. More weight should be attributed to the UVES results because the are based on spectra of higher resolution. Other literature determinations of the metal abundance of NGC 6441 are discussed in Paper II: they generally agree on a high metal abundance for this cluster.

It should be noted that the observed star-to-star scatter in Fe abundance is actually smaller than the estimate of the random errors. Hence, present data, from a wider sample than considered in Paper II, do not support the existence of a metal abundance spread in NGC 6441. Notably, there is no possible member of NGC 6441 that is significantly more metal-poor than the average abundance for the cluster. About 12% of the horizontal branch stars in NGC 6441 are on the blue side of the RR Lyrae instability strip, and an additional 4% are close to or within the instability strip (see Sect. 5 for a description of how we estimated these fractions): it could be claimed that these stars belong to a more metal-poor population. Clementini et al. (2005) have shown that the mean metallicity of the RR Lyrae of NGC 6441 is high, close to the mean value for the cluster. We may add here that the lack of any star more metal-poor than [Fe/H] = −0.6 in our sample of bona fide members of NGC 6441 (30 stars if we include also the stars observed with UVES) excludes at the 99% level of confidence the existence of a population of metal-poor stars as large as 16% of the cluster population (the total number of HB stars bluer than red HB). We may also exclude at 97% level of confidence a metal poor population accounting for 12% of the stars, that is the fraction of blue HB stars over the total number of HB stars. While a small population of metal-poor stars, enough to justify the population of blue horizontal branch stars, may still be present in the cluster, it is clear that at least the cluster RR Lyrae must result from the evolution of stars with the typical abundance found for NGC 6441. We conclude that very likely the anomalous HB and the spread in color of the RGB of NGC 6441 are not related to a spread of abundance for the heavy elements. While the first is probably a manifestation of the second parameter problem, the second is likely due only to differential reddening and extensive contamination by field (bulge) stars.

4.4. Abundances for other elements

Table 6 lists the average cluster abundances for the individual elements. For each star and for each element, we give the number of lines used in the analysis, the average abundance, and the rms scatter of individual values. Abundances for the odd elements of the Fe group (Sc and V) were derived with consideration for the not negligible hyperfine structure of these lines (see Gratton et al. 2003b, for more details).

Average abundances for the cluster, as well as the rms scatter of individual values around this mean value, are given in Table 7. For comparison, we also give the values derived from analysis of the UVES spectra in Paper II. In general, the values for the scatter agree fairly well with those estimated in our error analysis.

The overall pattern of abundance of NGC 6441 is typical of a globular cluster, with a large excess of the α-elements. This excess is larger than usually found in stars of similar metallicity belonging to the thick disk, where values of [Mg/Fe] and [Si/Fe] of about ∼0.2 dex are generally found (Gratton et al. 2003c; Bensby et al. 2005; Soubiran & Girard 2005). This large excess of the α-elements suggests that the material from which the stars of NGC 6441 formed was enriched by massive core collapse SNe, with little if any contribution by type Ia SNe. This might suggests either a peculiar metal enrichment process, or a very old age for the cluster. Unfortunately, no accurate age derivation is yet available and such estimate would be anyway difficult to be derived, due to the impact of differential reddening.

5. The O-Na anticorrelation

The Na abundances were derived from the 6154–60 Å doublet alone; they include corrections for departures from LTE, following the treatment by Gratton et al. (1999). We prefer not to use the 5682–88 Å doublet, that is very strong in the spectra of the program stars, because these lines are heavily saturated, contaminated by blends at the resolution of Giraffe spectra, and affected by large deviations from LTE. Additionally, the *S/N* of the spectra obtained with the HR11 grating is much lower than those obtained with HR13 grating, so that addition of the 5682–88 Å doublet data does not improve our Na abundances.

Telluric absorption lines were removed from the spectra in the region around the [OI] lines. No attempt was made to remove the strong auroral emission line; due to the combination of the Earth and stellar motions at the epoch of observations, the auroral emission line typically is at a wavelength about 0.7 Å blueward of the stellar line, so that it only occasionally disturbs its profile at the resolution of the Giraffe spectra. The O abundances were derived from equivalent widths: and confirmed by spectral synthesis. We did not apply any correction for either the blending with the Ni I line at 6300.339 Å, or for formation of CO. The NiI line is expected to contribute about 4 mÅ to the *EW* of the [OI] line, using the line parameters by Allende Prieto et al. (2001); the corresponding correction to O abundances is about 0.05 dex downward. CO coupling should be strong at the low effective temperature of the program stars. Unfortunately, the abundance of C is not determined. However, we expect that C is strongly depleted in stars near the tip of the RGB, with expected values of [C/Fe] ∼ −0.6 (Gratton et al. 2000). If the C abundance follows the Fe one in unevolved stars (as usually observed in metal-rich environments: see e.g. Gratton et al. 2000), we expect typical values of [C/O] ∼ −0.8 for stars in NGC 6441, in agreement with the non-detection of the C_2 lines in the spectral range 5610–30 Å. Neglecting CO formation, we could have underestimated the O abundances from forbidden lines by ∼0.05 dex. These two corrections should then roughly compensate, anyway they are within the error bars of the present determinations.

Abundances of O and Na are listed in Table 4. The [Na/Fe] ratio as a function of [O/Fe] ratio is displayed in Fig. 5, where we also plotted (with different symbols) the results obtained from the UVES spectra in Paper II. Overplotted is the mean line for several GCs (see Carretta et al. 2006). The usual Na-O anticorrelation seen in several other GCs is also evident in NGC 6441. Most of the red giants of NGC 6441 have rather high O abundances, but there exists a substantial fraction of O-poor, Na-rich stars. The Na abundances observed in the O-poor stars

Table 6. Average abundances for NGC 6441.

Star ID		[Mg/Fe]			[Si/Fe]			[Ca/Fe]			[Sc/Fe]			[Ti/Fe]
6005198	2	0.28	0.08	7	0.56	0.46	4	−0.02	0.16	5	0.05	0.18	1	0.48
6005934	3	0.26	0.22	7	0.50	0.33	4	0.31	0.31	5	0.10	0.14	1	0.12
6007741	2	0.44	0.33	1	0.60		3	0.40	0.06	2	0.38	0.22		
6010149	1	0.35		5	0.53	0.32				2				
6012768	2	0.13	0.10	2	0.32	0.03	4	0.13	0.19	2	−0.22	0.09	1	0.28
7004955	2	0.38	0.09	2	0.68	0.28	4	0.43	0.18	2	0.25	0.17	1	0.60
7006255	3	0.14	0.36	7	0.22	0.18	3	0.18	0.18	5	0.12	0.18	1	0.17
7006305	3	0.54	0.03	7	0.38	0.27	4	0.35	0.22	5	−0.14	0.18	1	0.39
7006319	3	0.50	0.18	7	0.45	0.18	4	0.24	0.19	5	0.28	0.12	1	0.38
7006354	2	0.32	0.08	2	0.57	0.12	4	0.05	0.28	2	−0.21	0.18	1	0.43
7006377	3	0.20	0.22	7	0.33	0.32	4	0.10	0.15	5	−0.02	0.16	1	0.07
7006470	3	0.35	0.27	7	0.24	0.22	3	0.17	0.15	4	−0.03	0.49	1	0.35
7006590	3	0.27	0.41	6	0.19	0.21	4	−0.13	0.22	5	0.10	0.22		
7006935	3	0.30	0.17	7	0.19	0.18	4	−0.03	0.16	5	−0.02	0.21	1	0.09
7006983	3	0.57	0.05	7	0.43	0.20	4	0.43	0.15	5	0.21	0.17	1	0.55
7007064	3	0.31	0.09	7	0.35	0.21	4	−0.16	0.21	5	−0.18	0.15	1	0.18
7007118	3	0.40	0.20	7	0.33	0.19	4	0.30	0.22	5	0.17	0.21	1	0.53
7007884	2	0.53	0.09	1	0.40		4	−0.05	0.22	2	0.07	0.27	1	0.05
7008891	2	0.33	0.07	2	−0.09	0.11	4	0.32	0.12	2	0.34	0.00	1	0.47
7013582	2	0.60	0.02	2	0.48	0.07	4	0.48	0.21	2	0.09	0.25	1	−0.03
8005158	2	0.49	0.09	2	0.65	0.07	4	0.15	0.38	2	−0.03	0.19	1	0.21
8005404	3	0.58	0.05	7	0.55	0.26	4	0.19	0.17	4	0.20	0.38	1	0.23
8006535	3	0.57	0.37	7	0.55	0.19	4	0.22	0.28	5	0.30	0.06	1	0.41
8008693				4	0.20	0.50	4	0.45	0.27	5	−0.02	0.10	1	0.58
8013657	2	0.31	0.06	2	0.68	0.03	4	0.37	0.19	2	−0.09	0.35	1	0.62

Star ID		[V/Fe]			[Cr/Fe]			[Ni/Fe]			[Ba/Fe]
6005198	10	−0.86	0.31	4	−0.32	0.49	13	0.15	0.22	1	0.20
6005934	9	−0.17	0.32	4	0.14	0.43	15	0.07	0.19	1	0.16
6007741				1	0.02		11	0.25	0.25	1	1.12
6010149	10	0.51	0.40	3	−0.05	0.20	4	0.39	0.26		
6012768							12	0.16	0.15	1	0.23
7004955				1	−0.13		12	0.25	0.25	1	0.31
7006255	10	−0.19	0.27	4	−0.17	0.24	15	0.05	0.26	1	0.04
7006305	11	−0.06	0.45	4	−0.20	0.37	15	0.36	0.27	1	0.11
7006319	11	0.35	0.28	4	0.08	0.23	16	0.02	0.27	1	0.09
7006354				1	0.20		11	0.14	0.23	1	0.19
7006377	10	−0.21	0.15	3	−0.46	0.17	16	0.10	0.20	1	0.01
7006470	6	−0.26	0.21	4	−0.23	0.11	15	0.27	0.28	1	0.13
7006590	11	−0.10	0.22	4	−0.20	0.29	15	−0.13	0.16	1	−0.24
7006935	11	−0.19	0.25	4	−0.29	0.13	16	−0.03	0.19	1	−0.18
7006983	11	0.08	0.22	4	−0.25	0.23	13	0.25	0.17	1	0.17
7007064	11	−0.14	0.25	4	−0.18	0.24	16	0.12	0.21	1	−0.01
7007118	11	0.06	0.32	4	−0.15	0.25	16	0.14	0.22	1	0.06
7007884				1	−0.13		11	−0.04	0.27	1	0.21
7008891				1	0.10		12	0.02	0.21	1	0.23
7013582				1	0.09		11	0.24	0.16	1	−0.08
8005158				1	−0.30		12	0.11	0.12	1	0.02
8005404	11	0.29	0.33	4	−0.17	0.19	14	−0.10	0.14	1	0.08
8006535	11	0.16	0.29	4	−0.20	0.43	15	0.17	0.20	1	0.14
8008693	10	−0.71	0.37	4	0.15	0.37	13	0.56	0.36	1	0.08
8013657				1	0.11		10	0.22	0.26	1	0.39

Table 7. Abundances for NGC 6441 members.

El.	This paper			Paper II	
	No. stars	[A/Fe]	rms	[A/Fe]	rms
Mg	24	+0.38	0.14	+0.34	0.09
Si	25	+0.41	0.19	+0.33	0.11
Ca	24	+0.21	0.19	+0.03	0.04
Sc	24	+0.07	0.17	+0.15	0.15
Ti	22	+0.33	0.20	+0.29	0.10
V	16	+0.01	0.24	+0.29	0.14
Cr	24	−0.11	0.18	+0.15	0.18
Ni	24	+0.13	0.13	+0.13	0.07
Ba	23	+0.10	0.14	+0.17	0.13

of NGC 6441 are very large, possibly larger than in other GCs. The distribution function of stars along the Na-O anticorrelation in NGC 6441 is shown in the lower panel of Fig. 6, where the ratio [O/Na] from our data is used. The histogram shows a a peak at rather large [O/Na] values, including about 2/3 of the stars, with an extended tail down to very low [O/Na] values, including the remaining one third of the stars.

We may compare this distribution of the [O/Na] values with the colors of the stars along the HB of NGC 6441 as shown in the HST CMD of the inner region of the cluster (Rich et al. 1997). We counted the cluster stars populating the three different parts of the HB, i.e. the blue HB, the RR Lyr instability strip and the

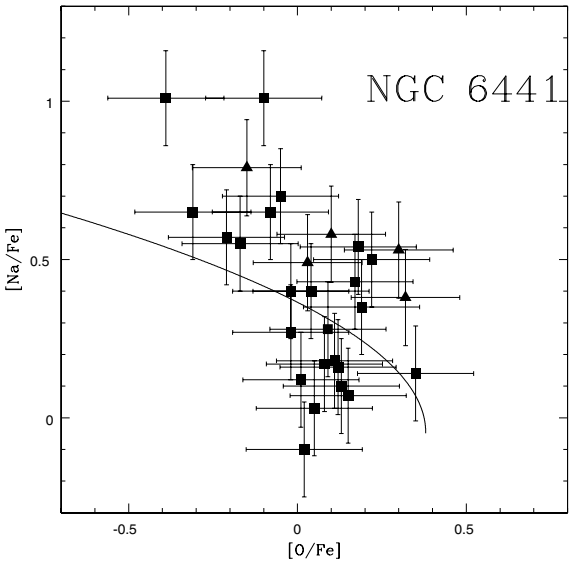

Fig. 5. [Na/Fe] vs. [O/Fe] abundance ratios for the stars adopted as member of the cluster. Triangles are objects observed with FLAMES-UVES (see Paper II), while squares are those of the present sample. The line represents the mean loci of the Na-O anticorrelation as derived from data of several GCs.

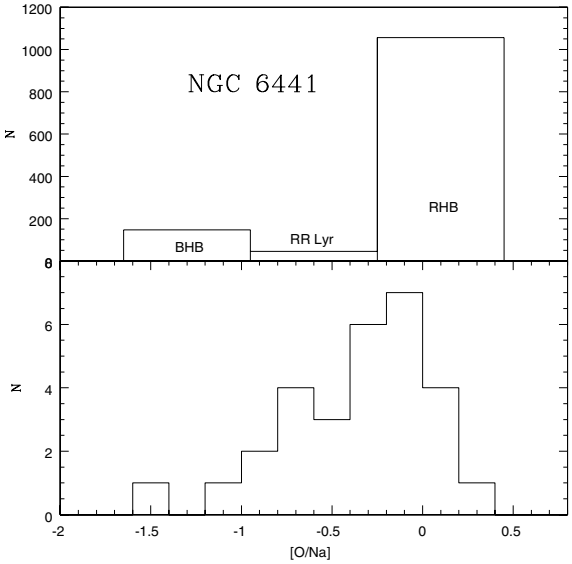

Fig. 6. *Upper panel* indicates the incidence of three different stars populations along the HB, selected from the CMD. *Lower panel* shows the distribution of the [O/Na] abundance ratios.

red HB. The areas of the CMD selected to represent each of the HB part are shown in Fig. 7. The final comparison is shown in the top panel of Fig. 6.

While this comparison is essentially qualitative (stars along the HB are binned in broad bins of colors, and both distributions have to be transformed into a mass distribution for the comparison to be really meaningful), the two distributions appear to be quite similar. About 3/4 of the RGB stars of NGC 6441 (21 out of 29) are O-rich and Na-poor, a fraction similar to the RHB over the total of HB stars (1056 out of 1248). Most of the remaining RGB stars have intermediate composition, with only one example of very low [O/Na] ratios. This should correspond to the population of HB stars of intermediate colors (possibly falling within the RR Lyrae instability strip), and to the tail including

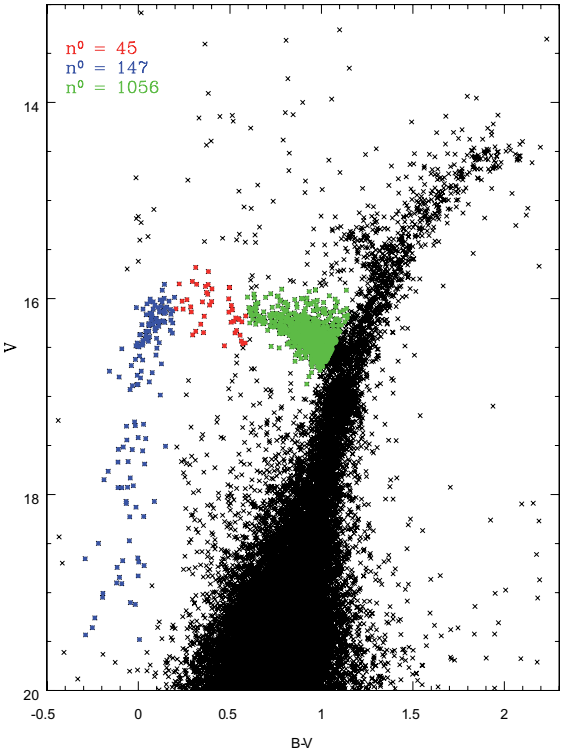

Fig. 7. Dereddened CMD diagram from HST data of the central region of NGC 6441 (Piotto et al. 2002). The different colors indicate the areas on the CMD in which the populations selected for the comparison can be found. *From top to bottom*: RR Lyr, blue HB, and red HB.

~15% of the stars on the blue part of the HB. Summarizing, the present data supports a qualitative agreement between the distribution of [O/Na] ratios for RGB stars and of colors along the HB of NGC 6441. This is in agreement with a scenario where the distribution of [O/Na] ratios in a GC reflects a distribution of He contents, and of masses of both RGB and HB stars.

6. The Ba-star #6007741

One member of NGC 6441, star #6007741, turned out to have a very strong Ba line (see Fig. 8). We measured *EW*s for a few additional lines of neutron capture element on the spectrum of this star; they are listed in Table 8. Table 9 lists the average abundances for the n-capture elements obtained from these *EW*s, along with the s-fraction (due to the main component of the s-process) in the Sun according to Käppeler et al. (1989, 1990a,b). The large overabundances of Ba and La (mainly s-process elements) and the much lower overabundances of the mainly r-process elements Nd and Eu, which are only slightly larger than those found in the remaining stars of NGC 6441 (see Paper II), identify this as an S-star. Figure 9 shows how well the abundance pattern of this star reproduces the abundances attributed to the main component of the s-process in the Sun for what concern the Ba-peak; however, we notice that the overabundances of Y and Zr are about two times smaller than the value expected from this distribution.

This abundance pattern strongly suggests that star #6007741 has been enriched by material processed during the thermal pulses phase of a small mass AGB star. The star itself is too faint for having experienced thermal pulses: the metallicity of NGC 6441 is similar to that of the LMC, and we know that in the LMC thermal pulses occur during the evolution of stars in

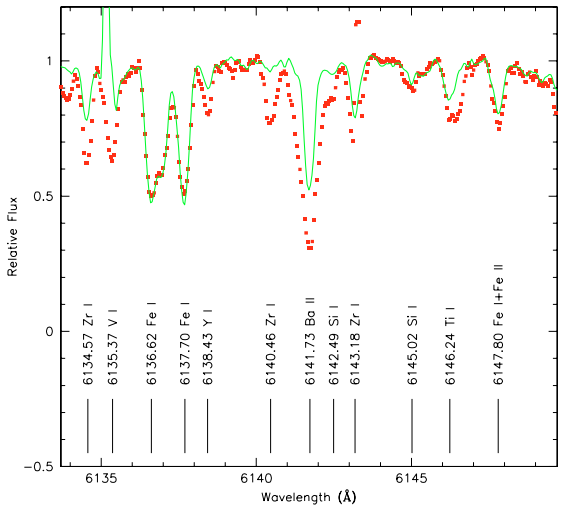

Fig. 8. Comparison between the spectrum of stars #6004471 (dots) and #7006935 (solid line) in the region of the Ba II line at 6141.73 Å. The two stars have similar atmospheric parameters. The first is characterized by much stronger lines of the n-capture elements.

Table 8. *EW*s for neutron capture element lines in the Ba-star #6007741 in NGC 6441.

Element	Wavelength (Å)	E.P. (eV)	log gf	Ref.	EW (mÅ)
Y I	6222.58	0.00	–1.70	1	78.0
Y II	5728.89	1.84	–1.12	1	50.0
Zr I	6127.46	0.15	–1.06	2	145.0
Zr I	6134.57	0.00	–1.28	2	134.0
Zr I	6140.46	0.52	–1.41	2	100.0
Zr I	6313.03	1.58	0.27	2	86.0
Ba II	6141.75	0.70	0.00	3	382.1
La II	5769.06	1.25	–0.69	4	88.0
La II	5797.57	0.24	–1.36	4	107.0
La II	6390.48	0.32	–1.41	4	90.0
Ce II	5613.69	1.42	–0.47	5	35.0
Nd II	5740.86	1.16	–0.53	6	54.0
Nd II	5804.00	0.74	–0.53	6	69.0
Nd II	5811.57	0.86	–0.86	6	50.0
Nd II	5825.86	1.08	–0.66	6	52.0
Nd II	6382.06	1.44	–0.75	6	46.0
Eu II	6313.03	1.28	–1.02	7	<20.0

1. Hannaford et al. (1982); 2. Biémont et al. (1981); 3. Holweger & Müller (1974); 4. Lawler et al. (2001b); 5. Biémont et al. (2005); 6. den Hartog et al. (2003); 7. Lawler et al. (2001a).

the approximate mass range $1.2 < M < 3\ M_{\odot}$, and with a luminosity of $-3.5 > M_{\rm Bol} > -6$ (Frogel et al. 1990). Hence, the abundance pattern observed in #6007741 is due to mass transfer from an originally more massive companion. Note that the system may have been disrupted after the mass transfer episode by close encounters with other cluster members, so it is not obvious that #6007741 should still have a companion. However, although the time span covered by our observations is quite limited, we detect a small variation in radial velocity for this object.

The donor star is expected to have produced also large amounts of C during He-shell flashes. We have derived the C abundance for star #6007741 using the spectral region 5610–5630 Å, which includes several lines of the 0–1 vibrational band of the C_2 Swan system. We compiled a line list for this spectral region from Kurucz (1992); for C_2, we used the line list from Phillips & Davis (1968), the electronic oscillator strength

Table 9. Abundances for neutron capture elements in the Ba-star #6007741 in NGC 6441.

Element	No. lines	[A/Fe]	rms	Solar fraction (main component of the s-process)
[Y/Fe] I	1	+0.84		0.81
[Y/Fe] II	1	+0.64		0.81
[Zr/Fe] I	4	+0.57	0.18	0.66
[Ba/Fe] II	1	+1.12		0.89
[La/Fe] II	3	+1.19	0.32	0.75
[Ce/Fe] II	1	+0.93		0.78
[Nd/Fe] II	5	+0.73	0.28	0.45
[Eu/Fe] II	1	<+0.93		0.07

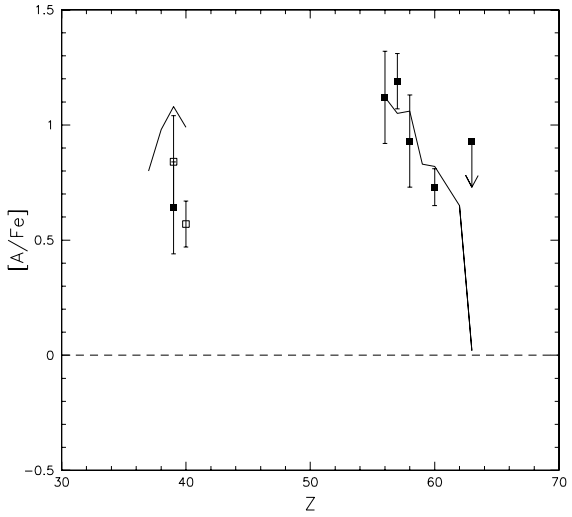

Fig. 9. n-Capture elements abundances with respect to iron measured in star #6007741. The line indicates the scaled s-process solar pattern. The Eu abundance shown is an upper limit. Open symbols are abundances from neutral lines; filled symbols from singly ionized lines.

from Lambert (1978), the Franck-Condon factor from Dwivedi et al. (1978), and the Hönl-London factors from Schadee (1964). We verified that a synthetic spectrum computed with this line list gives a very good fit to the solar spectrum for the standard solar C abundance. We then computed synthetic spectra appropriate for #6007741, and compared this spectrum with observations. In spite of the rather low *S/N* of the spectra, C_2 lines were clearly detected in the spectrum of star #6007741 (see Fig. 10); the best fit is obtained with a C/O ratio of 0.87 ± 0.10 (there is a strong coupling between C and O abundances through formation of CO at the temperature of this star). Since it is expected that C is strongly depleted in bright RGB stars of GCs (and this indeed occurs for the other program stars, where no C_2 lines are detectable: see for instance the case of star #7006935 shown in the same Fig. 10), we conclude that #6007741 has an anomalously high C abundance. While we have not observed the G-band of this star, we might predict that #6007741 should have a rather strong G-band, and should then be classified as a mild CH-star.

Ba and CH-stars are rare in globular clusters (for a catalogue, see Bartkevicius 1996). Most of them are in GCs of low central concentration. The rarity of Ba and CH-stars in GCs might be related with the high probability that primordial binaries with the right separation to form Ba and CH-stars (McClure et al. 1980; McClure 1984) are destroyed in the dense environments of GCs. It was quite unexpected to find such a star in NGC 6441, that is a quite strongly concentrated GC (c = 1.85: Harris 1996).

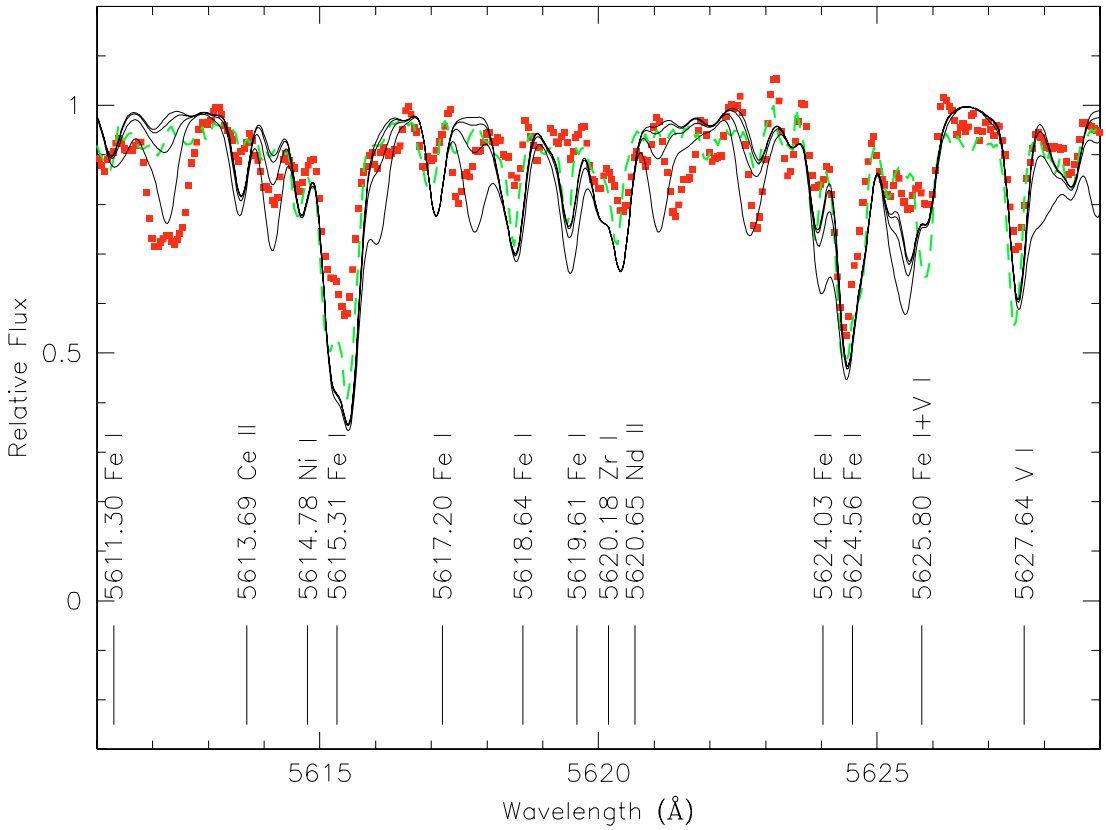

Fig. 10. Synthesis of the C_2 Swan band in the 5610–5630 Å wavelength range for star #6007741 (dots). The spectrum of star #7006935 is also plotted for comparison (dashed line). Synthetic spectra (solid lines) were computed for atmospheric parameters appropriate to star #6007741, N and O abundances of [N/Fe] = 0.5 and [O/Fe] = 0, and C abundances of [C/Fe] = −0.2, 0, 0.2, and 0.3 dex respectively.

7. Conclusions

In this paper we have derived RVs, atmospheric parameters and elemental abundances for a number of red giants in the field of the globular cluster NGC 6441, observed with the FLAMES multifibre facility and the Giraffe spectrograph at VLT2. Membership of the stars was derived from location in the cluster, radial velocities, and taking into account their chemical composition: the final sample includes 25 stars that are likely members of the cluster (in addition to the 5 stars observed with the UVES spectrograph and discussed in Paper I). Atmospheric parameters were obtained from the photometry: temperatures were obtained from the 2MASS K magnitudes, exploiting an average $K-(V-K)$ relation valid for cluster stars. In this way we minimize the impact of differential reddening on abundances.

From the analysis of the Giraffe spectra we derived an average metallicity of [Fe/H] = −0.34 ± 0.02 ± 0.04 dex, slightly higher than the value obtained in Paper II from UVES data. There is no indication of star-to-star scatter larger than the observational errors. The possibility that the RR Lyrae and the blue HB stars (unexpected in such a metal rich cluster) are due to a population of metal poor objects can then be ruled out at a high level of confidence. The cluster is overabundant in the α-elements Mg, Si, Ca, and Ti, indicating enrichment by massive core collapse SNe.

We measured O and Na abundances for 24 stars from the forbidden [OI] lines at 6300.3, 6363.8 Å and the Na doublet at 6154–60 Å. Combining this data with those extracted from UVES spectra (Paper II), O and Na abundances are available for 29 stars. The [Na/Fe] versus [O/Fe] ratios follow the well known Na-O anticorrelation, signature of proton-capture reactions at high temperatures, found in all other GCs examined so far. The distribution function of stars in [O/Na] (i.e. along the Na-O anticorrelation) is dominated by O-rich, Na poor stars, which constitute about 70% of the cluster stars, with a tail toward lower O and higher Na abundances. This distribution appear to be similar to the color distribution of stars along the HB, dominated by a well populated RHB, but with a significant tail of bluer stars. Adequate modelling is required to show whether qualitative agreement corresponds indeed to a quantitative one. This on turn should likely require an age determination for NGC 6441.

One of the star (#6007741) turned out to be a Ba-star, a class of objects that is relatively rare in globular clusters. The distribution of elements around the Ba-peak reproduces well the abundance pattern expected for the main component of the s-process; the lighter elements Y and Zr are however less overabundant by about a factor of two. Star #6007741 also has a rather high C abundance (the C/O factor is close to 1), in agreement with a scenario where the overabundance of s-process elements is due to mass transfer from a thermally pulsing small mass AGB star.

Acknowledgements. This research has been funded by grant "Experimental Nucleosynthesis in Clean Environments" by INAF. This publication makes use of data products from the Two Micron All Sky Survey, which is a joint project of the University of Massachusetts and the Infrared Processing and Analysis Center/California Institute of Technology, funded by the National Aeronautics and Space Administration and the National Science Foundation

References

Allende Prieto, C., Lambert, D. L., & Asplund, M. 2001, ApJ, 556, L63
Alonso, A., Arribas, S., & Martinez-Roger, C. 1999, A&AS, 140, 261

Barklem, P. S., Piskunov, N., & O'Mara, B. J. 2000, A&AS, 142, 467
Bartkevicius, A. 1996, Baltic Astron., 5, 217
Bensby, T., Feltzing, S., Lundström, I., & Ilyin, I. 2005, A&A, 433, 185
Biémont, E., Grevesse, N., Hannaford, P., & Lowe, R. M. 1981, ApJ, 248, 867
Biémont, E., Palmeri, P., & Quinet, P. 2005, Database on Rare Earths At Mons University, in http://w3.umh.ac.be/astro/dreams.html
Bragaglia, A., Carretta, E., Gratton, R. G., et al. 2001, AJ, 121, 327
Cardelli, J. A., Clayton, G. C., & Mathis, J. S. 1989, ApJ, 345, 245
Carretta, E., Bragaglia, A., Gratton, R. G., et al. 2006, A&A, 450, 523
Carretta, E., Bragaglia, A., Gratton, R. G., Lucatello, S., & Momany, Y. 2007, A&A, 464, 927
Cayrel, R. 1988, in The Impact of Very High *S/N* Spectroscopy on Stellar Physics, ed. G. Cayrel de Strobel, & M. Spite (Dordrecht: Kluwer Academic Publishers), IAU Symp., 132, 345
Charbonnel, C. 1994, A&A, 282, 811
Clementini, G., Gratton, R. G., Bragaglia, A., et al. 2005, ApJ, 630, L145
Côté, P. 1999, AJ, 118, 406
D'Antona, F., & Caloi, V. 2004, ApJ, 611, 871
D'Antona, F., Bellazzini, M., Caloi, V., et al. 2005, ApJ, 631, 868
De Angeli, A., Piotto, G., Cassisi, S., et al. 2005, AJ, 130, 116
den Hartog, E. A., Lawler, J. E., Sneden, C., & Cowan, J. J. 2003, ApJS, 148, 543
Denisenkov, P. A., & Denissenkova, S. N. 1990, Sov. Astron. Lett., 16, 275
Dubath, P., Meylan, G., & Mayor, M. 1997, A&A, 324, 505
Dwivedi, P. H., Branch, D., Huffaker, J. N., & Bell, R. A. 1978, ApJS, 36, 573
Frogel, J. A., Mould, J., & Blanco, V. 1990, ApJ, 352, 96
Gratton, R. G., Carretta, E., Eriksson, K., & Gustafsson, B. 1999, A&A, 350, 955
Gratton, R. G., Sneden, C., Carretta, E., & Bragaglia, A. 2000, A&A, 354, 169
Gratton, R. G., Bonifacio, P., Bragaglia, A., et al. 2001, A&A, 369, 87
Gratton, R. G., Bragaglia, A., Carretta, E., et al. 2003a, A&A, 408, 529
Gratton, R. G., Carretta, E., Claudi, R., Lucatello, S., & Barbieri, M. 2003b, A&A, 408, 529
Gratton, R. G., Carretta, E., Desidera, S., et al. 2003c, A&A, 406, 131
Gratton, R. G., Sneden, C., & Carretta, E. 2004, ARA&A, 42, 385
Gratton, R. G., Bragaglia, A., Carretta, E., et al. 2006, A&A, 455, 271 (Paper II)
Hannaford, P., Lowe, R. M., Grevesse, N., Biemont, E., & Whaling, W. 1982, ApJ, 261, 735
Harris, W. E. 1996, AJ, 112, 1487
Holweger, H., & Müller, E. 1974, Sol. Phys., 39, 19
Illingworth, G. 1976, ApJ, 204, 73
Käppeler, F., Beer, H., & Wisshak, K. 1989, Rep. Progr. Phys., 52, 945
Käppeler, F., Gallino, R., Busso, M., Picchio, G., & Raiteri, C. M. 1990a, ApJ, 354, 630
Käppeler, F., Zhao, W. R., Beer, H., & Ratzel, U. 1990b, ApJ, 355, 348
Kurucz, R. L. 1992, in The Stellar Populations of Galaxies, ed. B. Barbuy, & A. Renzini (Dordrecht: Kluwer Academic Publishers), IAU Symp., 149, 225
Lambert, D. L. 1978, MNRAS, 182, 249
Langer, G. E., Hoffman, R., & Sneden, C. 1993, PASP, 105, 301
Lawler, J. E., Bonvallet, G., & Sneden, C. 2001a, ApJS, 556, 452
Lawler, J. E., Wickliffe, M. E., den Hartog, E. A., & Sneden, C. 2001b, ApJS, 563, 1075
Layden, A. C., Ritter, L. A., Welch, D. L., & Webb, T. M. A. 1999, AJ, 117, 1313
Magain, P. 1984, A&A, 134, 189
McClure, R. D. 1984, ApJ, 280, 31
McClure, R. D., Fletcher, J. M., & Nemec, J. M. 1980, ApJ, 238, 35
Moehler, S., & Sweigart, A. V. 2006, A&A, 455, 943
Pasquini, L., Avila, G., Belcha, A., et al. 2002, Messenger, 110, 1
Phillips, J. G., & Davis, S. P. 1968, The Swan System of the C_2 Molecule (Berkeley: Un. California Press)
Pietrinferni, A., Cassisi, S., Salaris, M., & Castelli, F. 2004, ApJ, 612, 168
Piotto, G., King, I. R., Djorgovski, S. G., et al. 2002, A&A, 391, 945
Pritzl, B. J., Smith, H. A., Catelan, M., & Sweigart, A. V. 2001, AJ, 122, 2600
Rich, R. M., Sosin, C., Djorgovski, S. G., et al. 1997, ApJ, 484, 25
Rosenberg, A., Saviane, I., Piotto, G., & Aparicio, A. 1999, AJ, 118, 2306
Schadee, A. 1964, BAN, 17, 311
Skrutskie, M. F., Cutri, R. M., Stiening, R., et al. 2006, AJ, 131, 1163
Soubiran, C., & Girard, P. 2005, A&A, 438, 139
Sweigart, A. V., & Catelan, M. 1998, ApJ, 501, L63
Sweigart, A. V., & Mengel, J. G. 1979, ApJ, 229, 624
Tiede, G. P., & Terndrup, D. M. 1997, AJ, 113, 321
Valenti, E., et al. 2007, in preparation